Flow, Hydraulics, and Turbulent Mixing Over Kaena Ridge, Hawaii

by M.C. Gregg[1], G.S. Carter[2], and M.H. Alford[3]

[1] *School of Oceanography and Applied Physics Laboratory, University of Washington*

[2] *Department of Oceanography, University of Hawaii at Manoa*

[3] *Scripps Institution of Oceanography, University of California at San Diego*

Technical Report

APL-UW TR 2308

November 2023

Applied Physics Laboratory University of Washington

1013 NE 40th Street Seattle, Washington 98105-6698

Acknowledgments

We are indebted to the AMP and SWIMS crews for their persistence and skill at sea and to the National Science Foundation for funding. We also thank Mark Merrifield, who supported the senior author with a fellowship at the University of Hawaii.

ABSTRACT

Measurements with a depth-cycling towed body and microstructure profilers address several important issues left unanswered by previous results from the Hawaii Ocean Mixing Experiment (HOME) in 2000 and 2002. HOME sought to understand the energetics of surface tides being converted to internal tides and turbulence in gaps along the Hawaiian Ridge. Measurements in 2002 focused on Keana Ridge in the Kauai Channel, the most accessible of the three major sites. Here, we demonstrate that horizontal kinetic energy (*HKE*) at the shallow end of the ridge was strongly concentrated close to the bottom, below previously reported observations. We also show where and when internal modes were hydraulically controlled and that dissipation measurements must include the thin bottom boundary layer to obtain accurate energy balances over the ridge.

1. INTRODUCTION

Surface tides flowing through gaps in the Hawaiian Ridge produce strong local turbulence in addition to generating internal tides that transport energy away from the ridge as horizontally coherent waves detectable from satellites (*Ray and Mitchum*, 1996). Most of the energy conversion occurs at three sites: French Frigate Shoals, around the island of Nihoa, and in the Kauai Channel. Owing to the importance of these energy conversions, the Hawaiian Ocean Mixing Experiment (HOME) conducted an extensive multi-ship survey in 2000, termed HOME00, making measurements at the three sites that verified model predictions of internal tide generation (*Merrifield and Holloway*, 2002).

In 2002 HOME02 made intensive measurements of tidal conversion and dissipation in the Kauai Channel (*Rudnick et al*., 2003). Here, we demonstrate that horizontal kinetic energy (*HKE*) at the shallow end of the ridge was strongly concentrated close to the bottom, below previously reported observations. We also show where and when internal modes were hydraulically controlled and that dissipation measurements must include the thin bottom boundary layer to obtain accurate energy balances over the ridge.

Home02

The observations concentrated on Kaena Ridge. The northwest projection of Oahu, the ridge extends underwater half way across the Kauai Channel as it descends steeply from Kaena Point to a depth of 1,000 m and widens to form a relatively flat top with a 400-m-high seamount at the west end (**Fig. 1**). Barotropic tides forced up and over the steep sides of the ridge are the dominant source of strong internal tides generated in the channel.

Cross-ridge sections with a Sea Soar and a Doppler sonar observed beams of the M_2 internal tide crossing the crest from generation sites on the ridge flanks (*Cole et al*., 2009). Over the ridge, full-depth casts with Expendable Current Profilers (XCPs) and the Absolute Velocity Profiler (AVP) measured horizontal kinetic energy (*HKE*) much larger than the available potential energy (*APE*). Net fluxes were weak, however, leading *Nash et al.* (2006) to infer horizontally standing waves formed by at least two oppositely-directed waves. As the wave from the northern side propagated into deep water south of the crest, it formed a strong beam sloping upward from 200–300 m and a broader beam following the flank downward. The large momentum flux in the upward beam was also observed from the Floating Instrument Platform (R/P *FLIP*) moored at the southern edge of the ridge (*Pinkel et al*., 2012) and by repeated shipboard sections across the southern edge of the ridge (*Alford et al*., 2014).

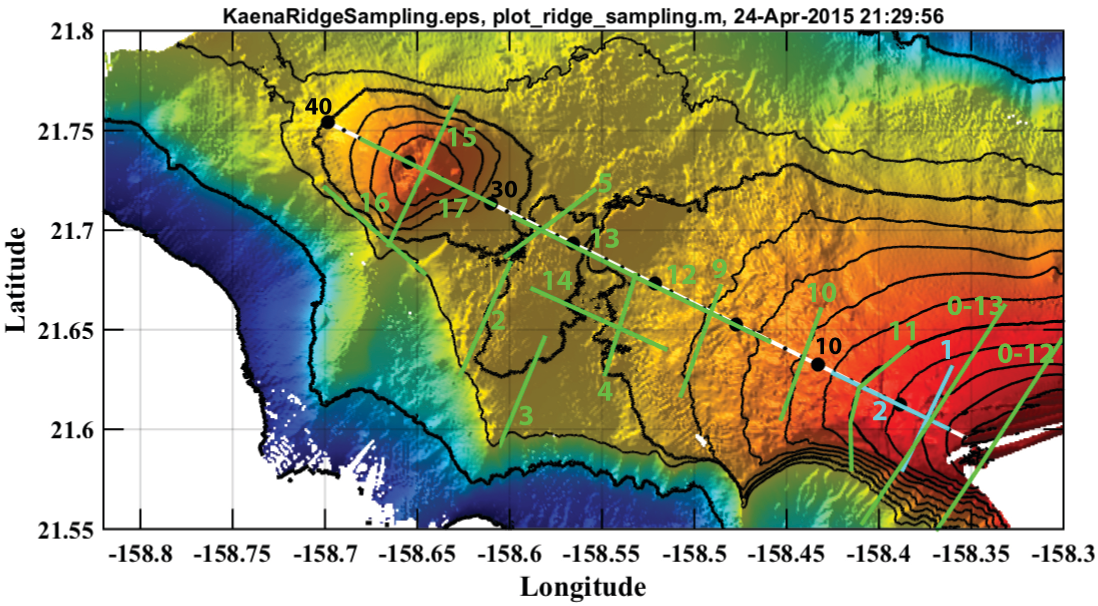

Figure 1. *Sampling over Kaena Ridge with AMP (green) and SWIMS (cyan) tracks overlaid on the bathymetry. Each sampling line was run for 25 h or 12.5 h and is identified by a group number. We reference positions on the ridge to the dashed white line along the axis from 21.5959°N, 158.3532°W to 21.7542°N, 158.6986°W. It is marked with small black dots at 1-km intervals from the east end, with larger dots at 5-km intervals. Two lines near the east end, labeled 1 and 2 colored cyan, were taken during HOME02 with SWIMS2 carrying upward and downward ADCPs. All others were taken with Deep AMPs during HOME02 except for groups 0-12 and 0-13 during HOME00.*

While sampling microstructure, *Carter and Gregg* (2006) found internal waves horizontally coherent with a frequency of $M_2/2$. Bicoherence analysis showed that those between depths of 525 and 595 m were nonlinearly coupled with the M_2 internal tide, indicating parametric subharmonic instability (PSI).

A synthesis of all HOME mixing data estimated net turbulent dissipation within 60 km of the ridge as $\varepsilon = 3 \pm 1.5$ GW, approximately 15% of the rate energy lost from the barotropic tide (*Klymak et al.,* 2006). In the upper half of the water column, average diapycnal diffusivity, K_ρ, was uniform at background intensity, 10^{-5} m^2 s^{-1}. In the lower half, specifically where $h/H > 0.55$, diffusivity increased with decreasing height, h, as $K_\rho = 10^{-5}\ 10^{1.18[1-(h/0.55H)]}$, where H is the total water depth. Inferences of mixing by *Cole et al.* (2009) from the Sea Soar and Doppler sections were of the same order-of-magnitude as the direct observations.

Using some of the observations in the *Klymak et al*. (2006) synthesis, *Carter et al.* (2006) and *Pickering and Alford* (2012) examined flow and mixing around and over the 400-m-high seamount near the west end of Kaena Ridge. Simulations showed tidal flows accelerating around the sides rather than passing over the top, and observations found dissipation rates higher on the northeast side and increasing near the bottom. The elevated mixing was attributed to the M_2 tidal beam generated on the north side of the ridge.

Simulations of tidal flows over steep bathymetry similar to Kaena Ridge revealed hydraulic jumps forming below the shelf break during maximum ebb tide (*Legg and Klymak*, 2008). As the flow reversed, the jumps evolved into internal bores propagating upslope with characteristics resembling features observed at R/P *FLI*P. These observations and simulations suggest that hydraulic responses may be important aspects of mixing over tall, steep bathymetry.

This Analysis

We extend *Klymak et al*. (2006), which reports bulk statistics of mixing at the ridge, by examining the structure of the flow and mixing, particularly at depths below the previous analysis. This is made possible using previously unreported observations from a depth-cycling towed body that came within a few meters of bottoms as deep as 600 m while carrying upward and downward ADCPs. Specifically, we:

1. Consider the structure of ε as well as of K_ρ.
2. Determine the structure of displacement, shear, and mixing along the ridge axis and across the southern side at the shallow end and where we have tracks shoreward of the seamount.
3. Examine hydraulic controls and their relation to mixing along and across the ridge.
4. Describe mixing in bottom boundary layers (BBLs), beginning with the AMP profile that hit bottom, to ask whether dissipation in BBLs is an important energy sink.

2. OBSERVATIONS

During HOME00 two microstructure sections were run with loosely-tethered AMP profilers across the shallow end of the ridge (0-12 and 0-13, and 0-18 along the same track as 0-13 in **Fig. 1**). Recognizing the inadequacy of the crude bathymetry available, we stopped profiling and began a survey with the R/V *Revelle* high-resolution mapping system. That bathymetry and some later measurements by Alan Chave were the basis for sampling in 2002 with SWIMS2 and AMP (**Fig. 2**). Most of those profiling tracks were run continuously for a full daily cycle.

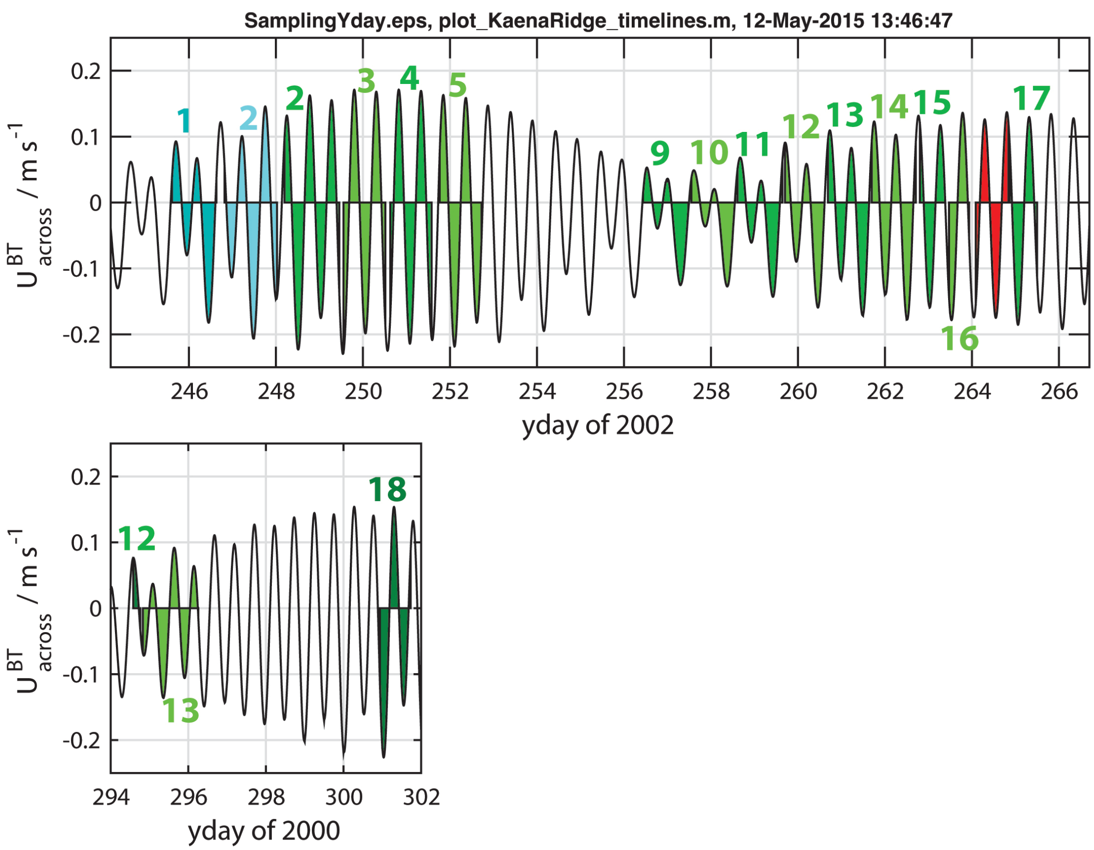

Figure 2. *Times of Kaena Ridge sampling overlaid on the cross-ridge barotropic current calculated with the sum of simulations individually forced by M2, S2, N2, K2, K1, O1, P1, or Q1 for the position where R/P FLIP was moored (21.6800, –158.6125). Colors match those in Fig. 1: green for AMP and cyan for SWIMS2. Alternating light and dark green distinguish successive AMP runs. The red group consisted of repeated runs back and forth along the ridge axis measuring currents with the 50-kHz HDSS. During HOME00 AMP groups 13 and 18 were run along the same waypoints.*

As described by *Miller et al*. (1989) and *Carter et al*. (2006), AMP carried airfoils, Fast Tip thermistors, a Neil Brown conductivity cell, and an altimeter that allowed profiling within a few meters of bottoms as deep as 1100 m. Most profiles, however, stopped 20 m above the bottom due to the reluctance of winch operators to suffer jibes from their shipmates when AMP hit bottom, which it did twice. The *Revelle* hydrographic Doppler ship's sonars (HDSS) (*Pinkel et al*., 2012) provided velocity and shear over most of the water column. One of the sonars operated at 140 kHz. The other, at 50 kHz, sampled every 8.6 m between 80 and 800 m with a trapezoidal window having a 25.8-m base. This analysis used the 50-kHz data.

The depth-cycling towed body SWIMS2 reached to 600 m carrying a 911+ Sea-Bird CTD and sensors for dissolved oxygen, chlorophyll, and optical backscatter. In addition, upward and downward 300-kHz ADCPs obtained velocity profiles throughout the full depth being sampled. An altimeter measured height when close to the bottom.

3. RIDGE CREST AVERAGES

Profiles

Stratification decreased exponentially from $N^2 = 10^{-4}$ m^2 s^{-1} at 100 m to 10^{-5} at 750 m, with means and medians overlaying tightly (**Fig. 3**). Below a thin, slight increase at 800 m, N^2 decreased another factor of two to the top of the BBL. Although ε was relatively uniform below 100 m, decreasing stratification amplified K_ρ below mid-depth to produce the exponential increase modeled by *Klymak et al*. (2006). Consistent with their approximately lognormal distributions, ε and K_ρ had means 2 to 20 times their medians.

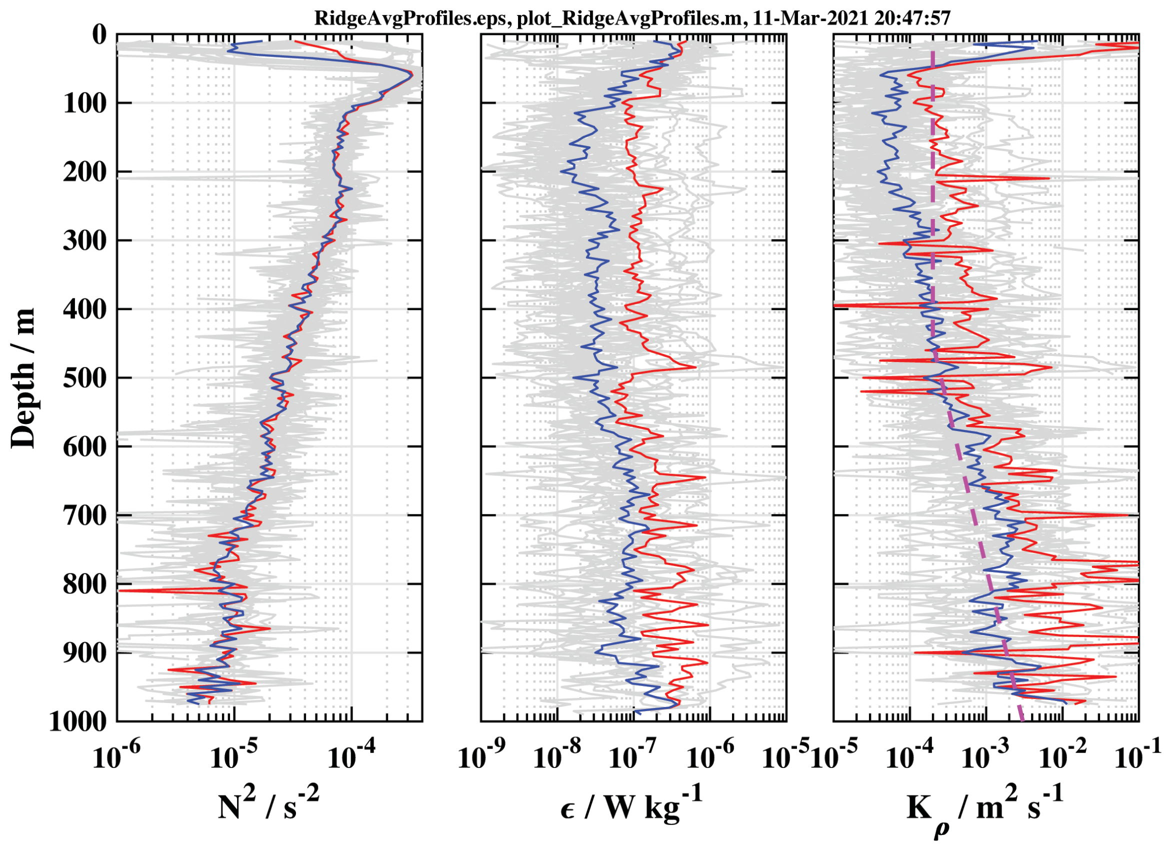

Figure 3. *All AMP and SWIMS profiles of stratification (N^2), turbulent dissipation rate (ε), and diapycnal diffusivity (K_ρ) over Kaena Ridge are plotted in gray. Overlays are arithmetic averages (red) and medians (blue). In addition, K_ρ is overlaid with the average diapycnal diffusivity for the Hawaiian Ridge (maroon dashed) formulated by Klymak et al. (2006). It is a better fit to the median than to the mean.*

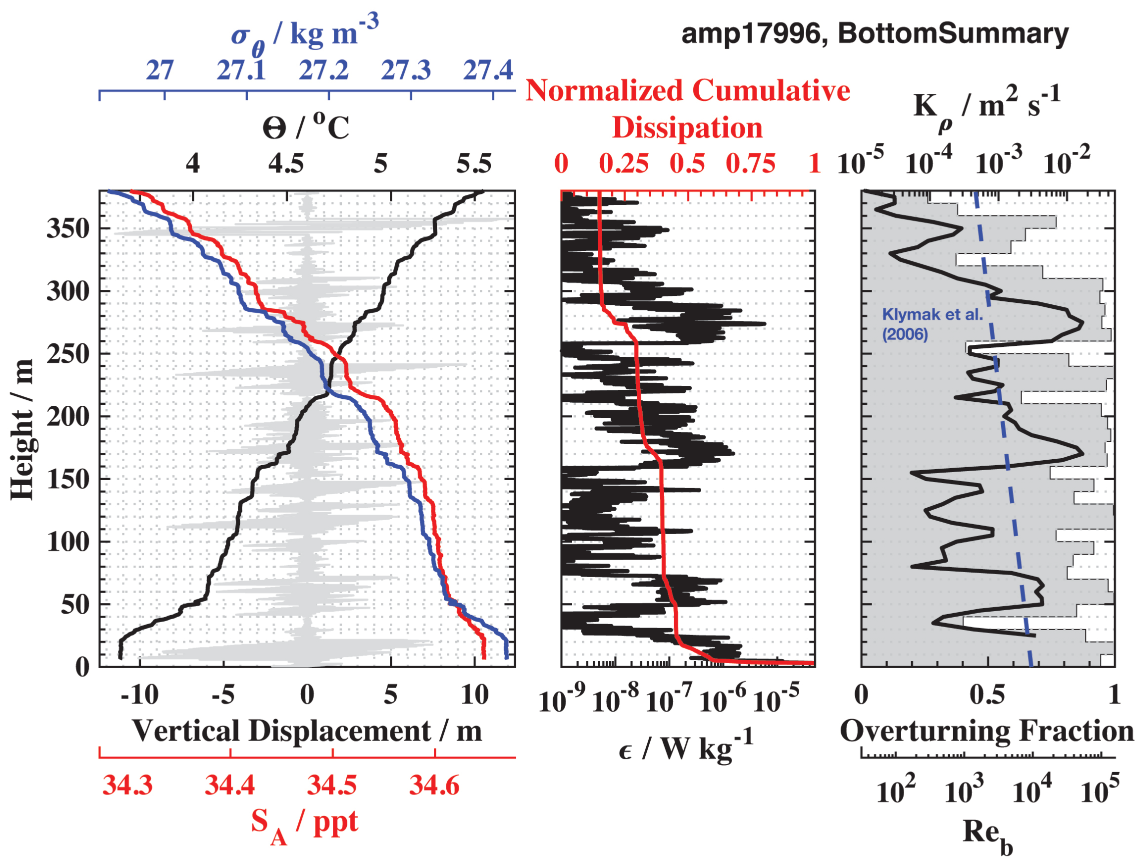

Figure 4. *Lower part of a profile that hit bottom at 23.4 km along the axis and 6.8 km south of it along cross-ridge track 3 (Fig. 1). Left) conservative temperature, absolute salinity, and potential density overlaid on Thorpe displacements (grey) computed from high-resolution temperature. Middle) Average ε (black) and its normalized cumulative sum below 100 m (red). Half of the total dissipation below 100 m was in the BBL, mostly due to the deepest value before impact. Right) K_ρ (solid) and the dissipation expression of Klymak et al. (2006) (dashed) are scaled on the top axis. The bottom axis gives the buoyancy Reynolds number estimated from the dissipation rate assuming constant kinematic viscosity and the ridge-average N^2. Shading shows the fractions of 10-m intervals that were in overturns (shaded).*

The increase of K_ρ toward the bottom appeared to be accompanied by nearly continuous overturning, as shown by the example profile in **Figure 4**. Owing to the absence of thermohaline intrusions well below the surface, overturns in SWIMS2 data were estimated from vertical displacements calculated by comparing observed temperature profiles with the same data sorted to decrease monotonically with depth

(*Thorpe*, 1977). The data were obtained from an FP07 thermistor sampled with an auto-ranging circuit to increase dynamic range. Overturns were defined where cumulative sums of displacements exceeded 10 mm, a value set by accumulating sensor noise. Even though overturns thinner than 0.1 m were ignored, overturns frequently exceeded 80% of profiles within a few hundred meters of the bottom. Overturns were much less common closer to the surface. Peak turbulent intensities with buoyancy Reynolds numbers, $Re_b \equiv \varepsilon / (\nu N^2)$, greater than 10^4 had overturn fractions > 90%.

Section Along the Axis

There was no discernible lateral trend in N^2 along the axis (**Fig. 5**), but vertical displacement variance, ζ^2, and horizontal kinetic energy, *HKE*, varied with distance from Kaena Point. At ≈ 10 to ≈ 30 km from the point, vertical displacements in weakly stratified water below 500 m were tenfold larger than those at shallow depth. The average downward decay in stratification greatly reduced these contrasts when displacements were scaled as potential energy density, $PE = N^2 \zeta^2$. Also, *PE* was minimal in the internal tide beam outlined by the oval (**Fig. 5d**). Horizontal kinetic energy, $HKE = ½ < U^2_{\text{cross-ridge}} >$, was largest in the lower part of the internal tide beam and in the bottom ≈ 100 m over the sloping bottom. (This strong bottom flow may have continued deeper than 600 m, the limit sampled by SWIMS2.)

Average dissipation rates were highest at the shallow end of the ridge and over the seamount (**Fig. 6**). Summing the vertical average across the section and normalizing, half of the net dissipation was over the seamount and a quarter was over the sloping bottom. Dissipation in the internal tide beam was minimal. Owing to weak stratification in the trough between the seamount and the shoreward slope, the corresponding diapycnal diffusivity was intensified near the bottom with $K_\rho \geq 10^{-3}$ m^2 s^{-1}, where shear variance was also large (**Fig. 7**).

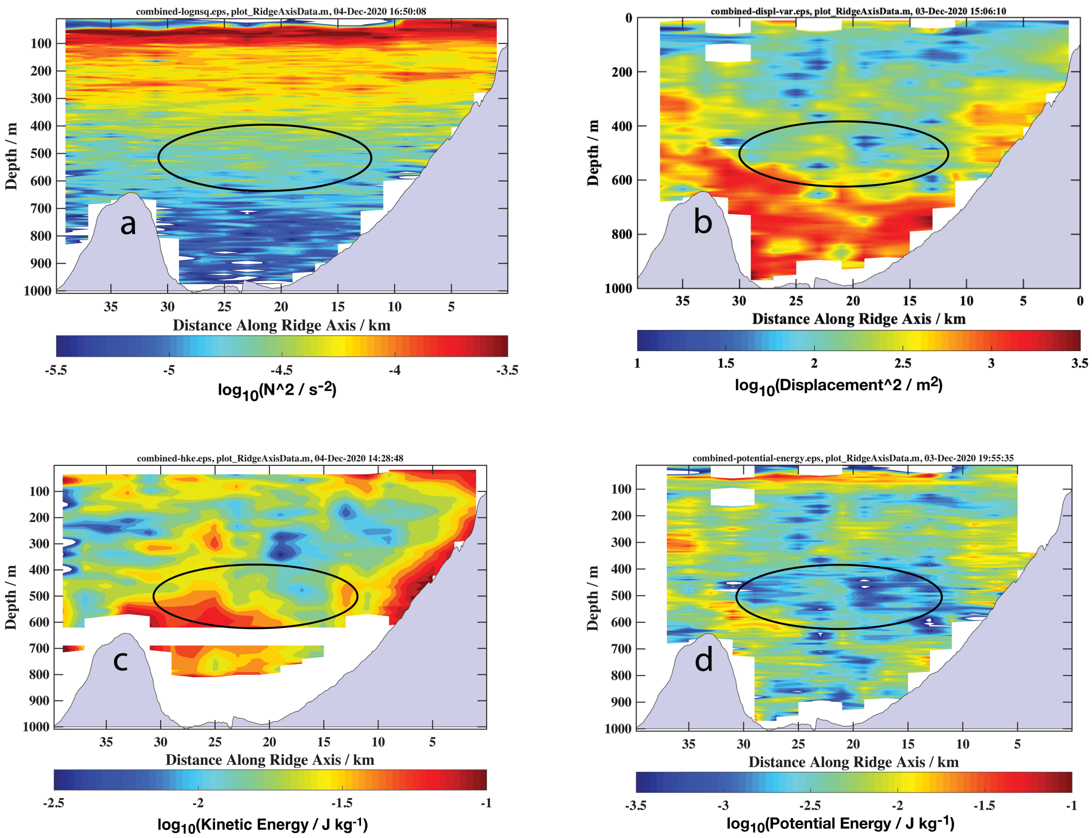

Figure 5. *Composite averages from SWIMS and standard shipboard profiling of a) stratification, b) vertical displacement variance, c) HKE, and d) vertical potential energy within ± 2 km of the ridge axis. SWIMS profiles measured velocity to the bottom as deep as 600 m at the shallow end. The gap in HKE between 600 and 700 m resulted from interference between the two ship-mounted profilers. Black ovals show the approximate center of cross-ridge internal tide beams inferred by Carter and Gregg (2006) from measurements by Martin et al. (2006).*

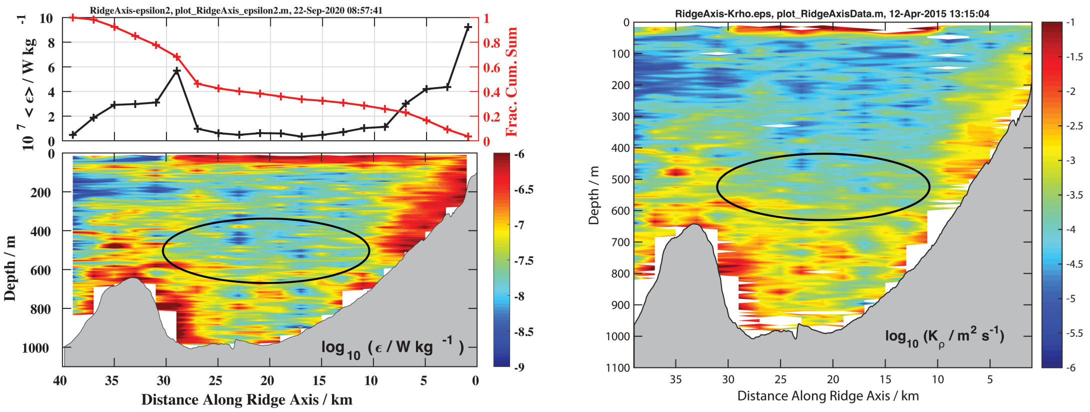

Figure 6. *Left, upper) Vertically-averaged ε (black) and its fractional cumulative sum (red) within ± 2 km of the ridge axis. Left, lower) Logarithm of average ε from airfoils on AMP and density overturns on SWIMS2. Right) Average diapycnal diffusivity, K_ρ.*

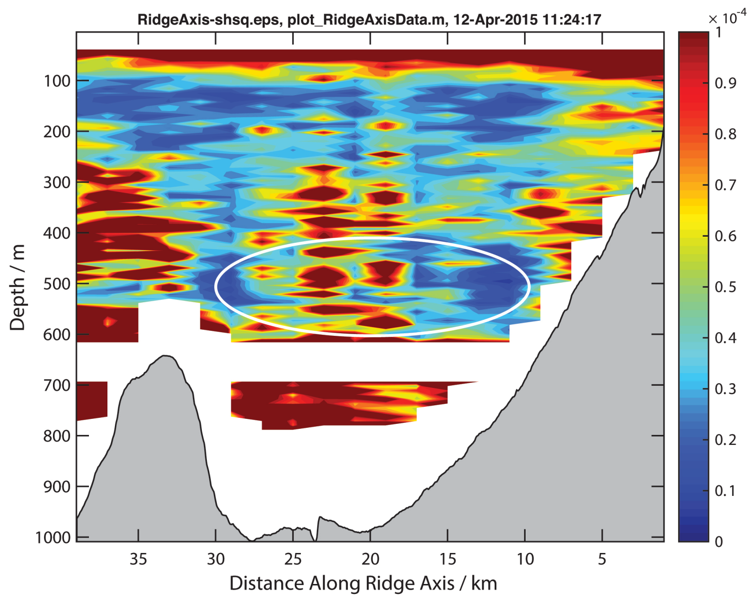

Figure 7. *Shear^2 estimated from the R/V Revelle 50-kHz Doppler sonar averaged over a tidal cycle.*

Bottom Boundary Layer

One of the two profiles that hit the seafloor contained intense turbulence, $\varepsilon \sim 10^{-5}$ W kg^{-1}, in a 20-m-thick BBL (**Fig. 4**). This thin section contributed half of the net dissipation below 100 m in the profile. The other bottom-hit, however, found no bottom increase, even though both profiles were within a mile of each other near times of maximum cross-ridge barotropic flow. Local variations in bottom roughness are likely responsible for the contrast in dissipation rates. Highly turbulent bottom layers cannot be assumed, but they should be examined in future measurements, as they may contribute a significant fraction of dissipation over the ridge.

Off-Axis Averages and Vertical Integrals

Off-axis dissipation rates were moderate, with averages of 10^{-7} to 10^{-8} W kg^{-1}, except around the seamount and across the shallow end of the ridge, where turbulence was more intense, with averages $\geq 10^{-6}$ (**Fig. 8**, left). Integrating vertically reveals that the shallow end dominated net dissipation. Owing, however, to the decrease in stratification with depth, diapycnal diffusivities were most intense around and over the seamount (not shown).

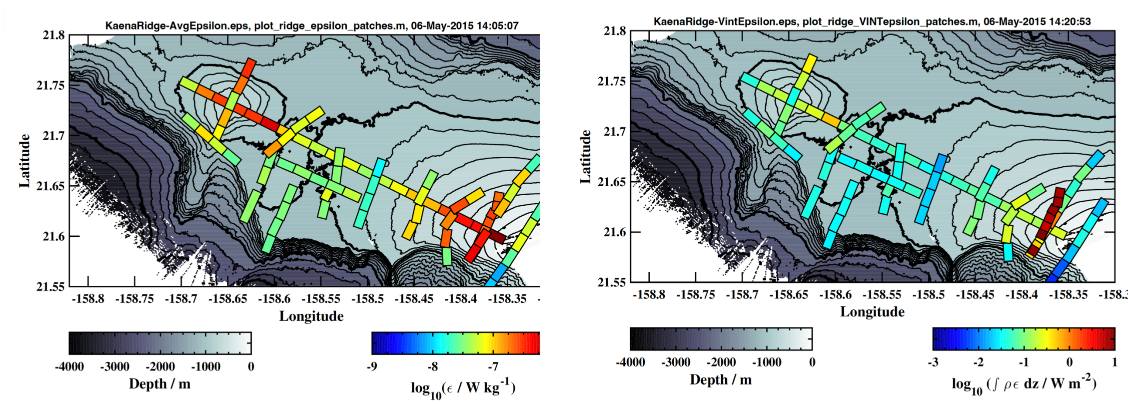

Figure 8. *Dissipation rates below 50 m averaged in time and vertically along sampling lines (left) and vertical integrals of time averages (right). Mixing was most intense along the axis, except for one cross-ridge line at the shallow end (right).*

4. HYDRAULIC CONTROLS AT THE SHALLOW RIDGE CREST

To investigate the role of hydraulic controls in producing the strong mixing over the shallow end of the ridge crest, phase speeds of long internal waves were calculated following *Pratt et al*. (2000) and *Gregg and Pratt* (2010). Phase speeds of internal modes occur in pairs with their magnitudes bounded by the slowest and fastest mean velocities. Modes propagating against the mean flow with the same magnitude are held to zero velocity relative to the bottom and are said to be hydraulically controlled, while those with faster phase speeds are considered supercritical, and ones with slower speeds are subcritical. The SWIMS2 along-ridge sections reveal modes 2 and higher being controlled at varying distances from Kaena Point when cross-ridge northward flow was strong (**Fig. 9**).

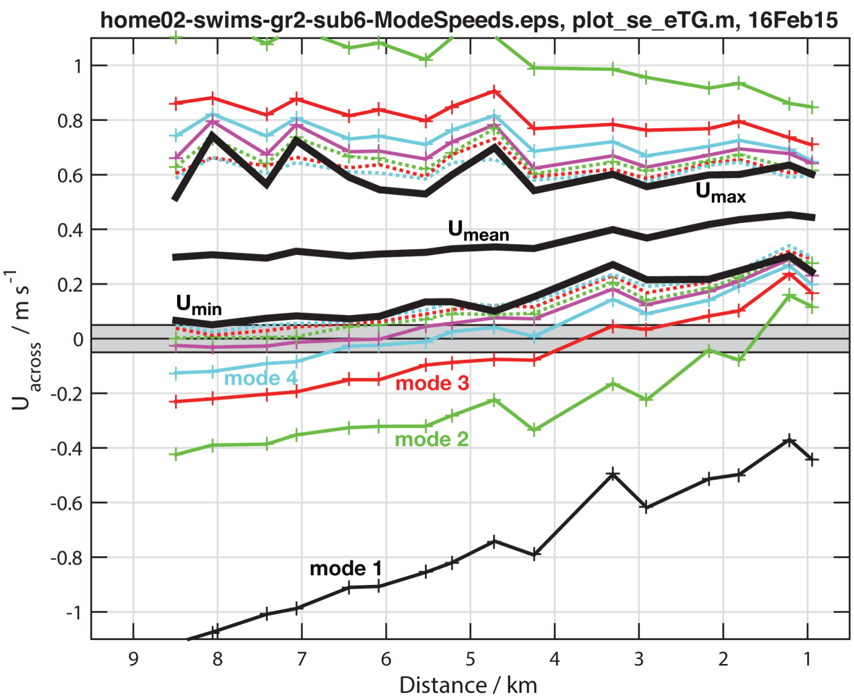

Figure 9. *Along-ridge section in 2002 from SWIMS2 during strong northward flow across the ridge. Thick black lines connect vertically-averaged cross-ridge velocities in each profile. Thin colored lines are calculated mode speeds. Modes higher than 5 are shown by dashed lines that asymptote to minimum or maximum average flow speeds. Shading between ± 0.05 m s^{-1} shows where internal modes are considered to be hydraulically controlled. Owing to shoaling depth, mode speeds decrease shoreward. Mode 2 was controlled shoreward of 2 km and was supercritical closer than 1.5 km. Control of mode 4 began at 6.7 km, and mode 5 and higher were controlled or supercritical throughout the measured section.*

Using the repeated SWIMS2 along-ridge runs to form pseudo time series at fixed positions shows that control was often brief, occurring only at peak flows during the tidal cycle and was more restricted to higher modes deeper along the ridge (**Figs. 10** and **11**). Dissipation rates show no apparent relation to these times of hydraulic control. Nor could we find patterns or statistical relations between times of control and ε in other SWIMS2 sections along or across the ridge.

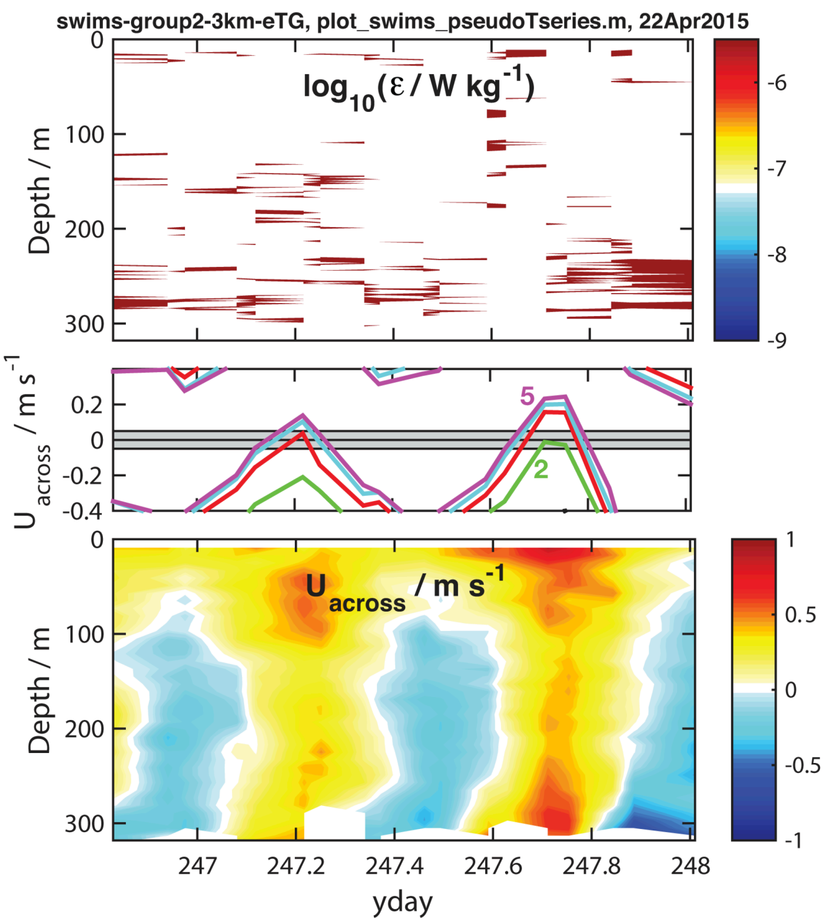

Figure 10. *Pseudo time series at 3 km along the ridge axis. The top panel shows the dissipation rate, the middle panel has internal wave speeds for modes 2 (green) through 5 (maroon), and the bottom panel exhibits cross-ridge velocity versus depth. Modes 3 and higher were controlled during the first phase of northward flow. During the second northward phase, faster velocities controlled modes 2 and higher. The series was formed from the SWIMS2 runs back and forth along the ridge crest.*

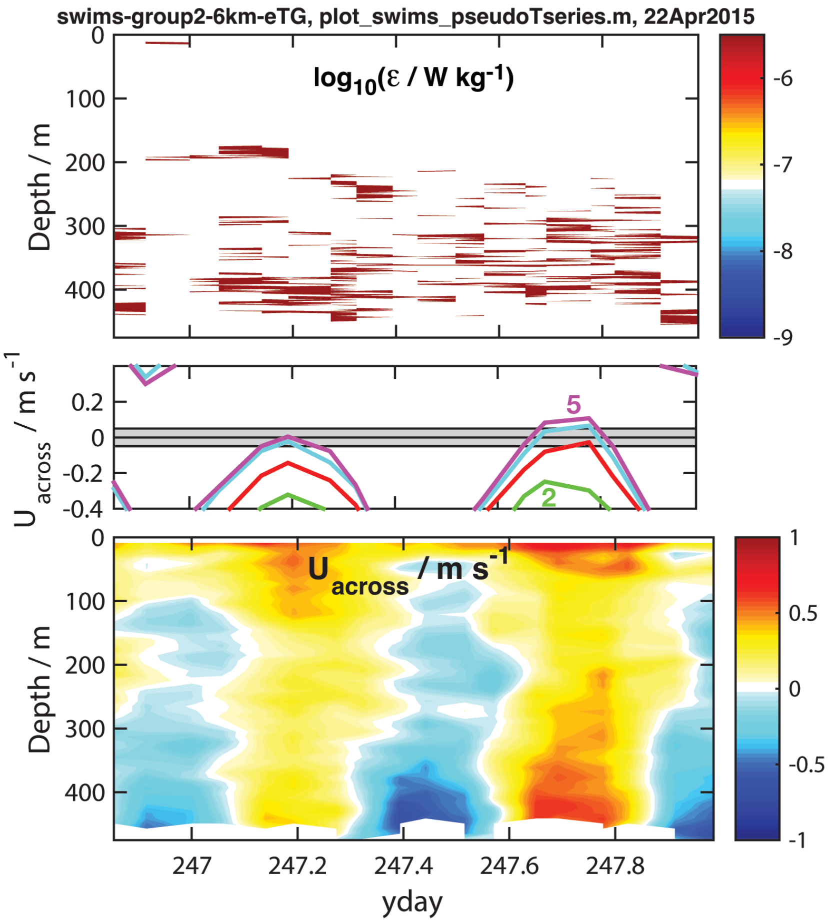

Figure 11. *Pseudo time series at 6 km in the same format as Fig. 10. At this deeper location, control was limited to higher modes than at 3 km.*

Across-ridge AMP sections from HOME00, however, contain signatures consistent with hydraulic disturbances (**Fig. 12**). No modes were controlled during moderate southward flow (left), but density was highly strained and dissipation was elevated in water spilling over the sill. During strong northward flow modes 2 and higher were controlled, and control likely would have been shown to be stronger if we could have measured velocity to the bottom. Density showed strong overturns, and dissipation was intense below 100 m between cross-ridge distances of –1 to +3 km.

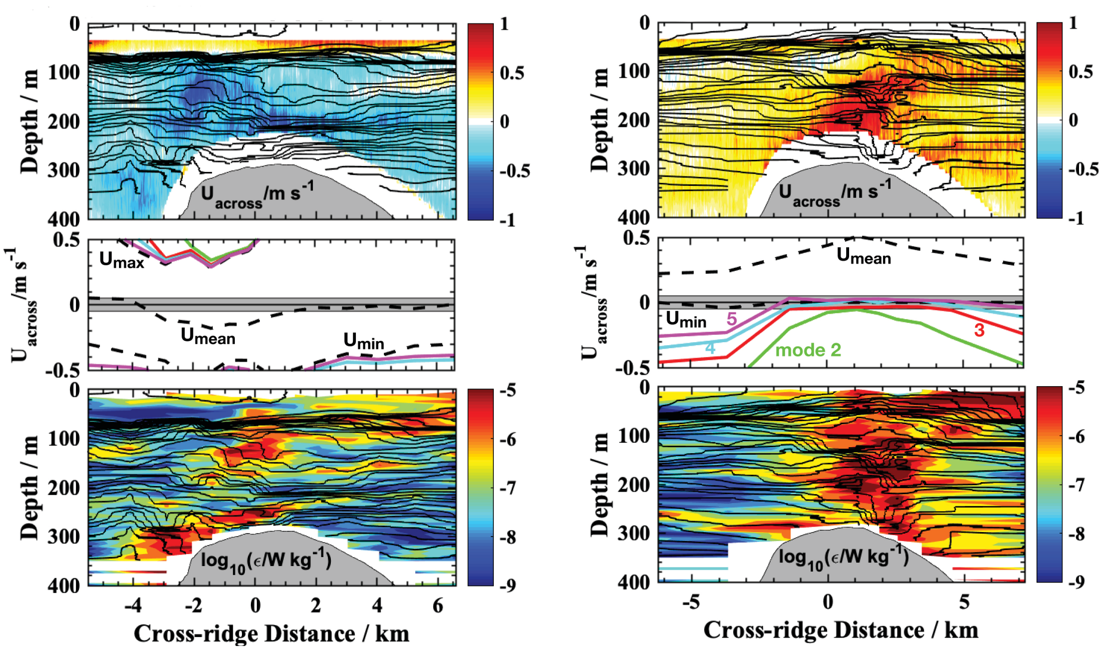

Figure 12. *Cross-ridge velocity, internal mode speeds, and dissipation rate from two AMP sections in 2000. Contours of potential density at 0.1 kg m^{-3} are overlaid on top and bottom panels. No modes were controlled during moderate southward flow (left), but the density field was also strongly strained in a depth band sloping downward past the ridge crest. During moderate northward flow (right), modes 2–5 were controlled, dissipation was high, and density exhibited large overturns a few kilometers downstream of the ridge crest.*

Higher modes were critical or supercritical throughout this section. The pseudo time series at 3 km shows critical and supercritical flow occurring only during several hours of each tidal cycle (**Fig. 10**). At 6 km controls did not last as long and involved higher modes (**Fig. 11**). Surprisingly, dissipation rates in the bottom 100 m are highest when northward velocity diminishes and baroclinic modes are subcritical.

5. SUMMARY

Repeated surveys along and across Kaena Ridge with AMP and SWIMS2 demonstrate that:

1. Internal modes 2 and higher were controlled for 1–2 h at the shallow end of the ridge during peak cross-ridge flow to the north. Deeper along the ridge control weakened as the ridge deepened with distance from Kaena Point. By 6 km, control of mode 2 was lost, and only modes 4 and 5 were briefly controlled during weaker peak flow.
2. Within 10 km of Kaena Point, the limit of our direct measurements to the bottom, *HKE* was concentrated in the bottom 100 m. Farther offshore, *HKE* was equally intense directly over the seamount and at least part of the ‘trough’ between the seamount and the sloping ridge.
3. Displacement variance was largest below 600 m in the ‘trough’, with values ≥ 1,000 m^2, but the signature in potential energy was modest owing to weak stratification. Potential energy had a weak minimum at depths of 400–600 m, where topographically-generated internal waves propagate across the ridge crest.
4. Turbulent dissipation rates were $\varepsilon \sim 10^{-6}$ W kg^{-1} within 100 m of the bottom to a depth of 600 m and over and along the flanks of the seamount. Integrated vertically, these contributed about 1/4 and 1/2 of the total dissipation over the ridge crest. The dissipation rates translated into diapycnal diffusivities, K_ρ, of $10^{-3} - 10^{-2}$ m^2 s^{-1}. Owing to the weak stratification below 600 m, the ‘trough’ was filled with comparable diffusivities.
5. One of the two profiles that hit bottom suggest that accurate estimates of total dissipation over the ridge cannot be made without thorough sampling of the BBL. Even excluding the ≈ 10^{-5} data point at the very bottom, the 20-m-thick BBL accounts for 10–15% of the cumulative fraction.
6. Overturns estimated from temperature profiles where thermohaline intrusions appear to be absent show more than half of the bottom 300 m overturning. This finding, however, must be considered tentative, as it was not made from density profiles free of salinity spiking.

6. REFERENCES

Alford, M., J. Klymak, and G. Carter, Breaking internal lee waves at Kaena Ridge, Hawaii, *Geophys. Res. Lett., 41*, 906–912, doi: 10.1002/2013GL059070, 2014.

Carter, G. S., and M.C. Gregg, Persistent near-diurnal internal waves observed above a site of M_2 barotropic-to-baroclinic conversion, *J. Phys. Oceanogr., 36*, 1136–1147, 2006.

Carter, G.S., M.C. Gregg, and M. Merrifield, Flow and mixing around a small seamount on Kaena Ridge, Hawaii, *J. Phys. Oceanogr., 36*, 1036–1052, 2006.

Cole, S., D. Rudnick, and B. Hodges, Observations of tidal internal wave beams at Kaui Channel, Hawaii, *J. Phys. Oceanogr., 39*, doi:10.1175/2008JPO3937.1, 2009.

Gregg, M., and L. Pratt, Flow and hydraulics near the sill of Hood Canal, a strongly sheared, continuously stratified fjord, *J. Phys. Oceanogr., 40*, 1087–1105, doi:10.1175/2010JPO43121, 2010.

Klymak, J., J. Moum, J. Nash, E. Kunze, J. Girton, G. Carter, C. Lee, T. Sanford, and M. Gregg, An estimate of tidal energy lost to turbulence at the Hawaiian Ridge, *J. Phys. Oceanogr., 36*, 1148–1164, 2006.

Legg, S., and J. Klymak, Internal hydraulic jumps and overturning generated by tidal flow over a tall steep ridge, *J. Phys. Oceanogr., 38*, 1949–1964, doi:10.1175/2008JPO03777.1, 2008.

Martin, J., D. Rudnick, and R. Pinkel, Spatially broad observations of internal waves in the upper ocean at the Hawaiian Ridge, *J. Phys. Oceanogr., 36*, 1085–1103, 2006.

Merrifield, M.A., and P.E. Holloway, Model estimates of M_2 internal tide energetics at the Hawaiian Ridge, *J. Geophys. Res., 107*, doi:10.1029/2001JC000996, 2002.

Miller, J., M. Gregg, V. Miller, and G. Welsh, Vibration of tethered microstructure profilers, *J. Atmos. Ocean. Technol., 6*, 980–984, 1989.

Nash, J., E. Kunze, C.M. Lee, and T.B. Sanford, Structure of the baroclinic tide generated at Kaena Ridge, Hawaii, *J. Phys. Oceanogr., 36*, 1123–1135, 2006.

Pickering, A., and M. Alford, Velocity structure of internal tide beams emanating from Kaena Ridge, Hawaii, *J. Phys. Oceanogr., 42*, 1039–1044, 2012.

Pinkel, R., L. Rainville, and J. Klymak, Semidiurnal baroclinic wave momentum fluxes at Kaena Ridge, Hawaii, *J. Phys. Oceanogr., 42*, 1249–1269, 2012.

Pratt, L., H. Deese, S. Murray, and W. Johns, Continuous dynamical modes in straits having arbitrary cross sections, with applications to the Bab al Mandab, *J. Phys. Oceanogr., 30*, 2515–2534, 2000.

Ray, G., and R. Mitchum, Surface generation of internal tides generated near Hawaii, *Geophys. Res. Lett., 23*, 2101–2104, 1996.

Rudnick, D., et al., From tides to mixing along the Hawaiian Ridge, *Science, 301*, 355–357, 2003.

Thorpe, S., Turbulence and mixing in a Scottish loch, *Proc. Roy. Soc. Lond. A, 286*, 125–181, 1977.